ECCOMAS Congress 2016
VII European Congress on Computational Methods in Applied Sciences and Engineering
M. Papadrakakis, V. Papadopoulos, G. Stefanou, V. Plevris (eds.)
Crete Island, Greece, 5–10 June 2016

A MULTIPHASE MODEL FOR THE NUMERICAL SIMULATION OF ICE-FORMATION IN SEA-WATER

Vanessa Covello[1], Antonella Abbà[1], Luca Bonaventura[2], Alessandro Della Rocca[2,3], and Lorenzo Valdettaro[2]

[1]Department of Aerospace Science and Technology, Politecnico di Milano
Via La Masa 34, 20156, Milano, Italy
e-mail: vanessa.covello, antonella.abba@polimi.it

[2] MOX-Modelling and Scientific Computing, Department of Mathematics, Politecnico di Milano
Via Bonardi 9, 20133, Milano, Italy
e-mail: luca.bonaventura, lorenzo.valdettaro@polimi.it

[3] Tenova S.p.A.
Via Albareto 31, 16135, Genova, Italy
e-mail: alessandro.dellarocca@tenova.com, alessandro.dellarocca@polimi.it

Keywords: ice modelling, multiphase flows, projection methods, finite volume method.

Abstract. *The first aim of this work is to improve the models currently available for the simulation of ice production in turbulent seawater, by means of the development of a multiphase model able to describe all the stages of ice production, overcoming the limitation of previous attempts, mainly based on Boussinesq approximation. We consider the mixture of ice and seawater as a dense compressible fluid, and we model the behaviour of seawater by an equation of state that links seawater density to temperature, salinity and pressure. The model is able to reproduce the interaction phenomena occurring between phases when the ice volume fraction exceeds the values allowed by the Boussinesq approximation, including in the momentum equations additional terms, related to the drag force between liquid and particles, and to the particle-particle interaction force. The second aim of our work is to implement and validate a numerical solver of our model. For this purpose, the model uses a sophisticated modelling approach, typically adopted for the numerical simulation of multiphase flows of industrial interest. The multiphase model can be coupled to the Large Eddy Simulation technique. The behaviour of the governing equations in the incompressible limit is investigated by means of a low-Mach number asymptotic analysis. The divergence constraint condition for the velocity field of continuous phase can then been imposed on the zero-Mach number equations by means of a projection method. The governing equations are discretized using the finite volume method, and the performance of the multiphase model has been assessed by solving a laminar Rayleigh-Bénard convection, for both large and small ice concentration regimes. In small concentration regime, the numerical solutions have been compared with the solutions obtained by a finite difference numerical code, based on the Boussinesq approximation.*

1 INTRODUCTION

Ice formation in the ocean is a complex phenomenon, whose correct description is essential in order to model adequately the atmosphere-ocean heat fluxes, the salt rejection phenomena and the damping effects related to the interactions among ice production, salt rejection and turbulent convection. The first stage of ice formation at the supercooled free surface of oceans, rivers and lakes is denoted as frazil-ice, a suspension of small individual randomly-oriented crystals, typically of 1 - 4 mm in diameter and 1 - 100 μ m in thickness [28, 31]. The frazil ice evolves rapidly into a thin slurry of ice platelets, known as grease ice. As cooling continues, the crystals freeze together into small disks called pancake-ice. Finally, during the last stage of sea ice evolution, the pankace-ice coalesces into a continuous ice sheet.

In this work, we focus our attention on the initial stages of ice production, frazil and grease ice. It is well known that ice formation greatly affects the geophysical and biological processes occurring in the polar oceans and that the subsequent salt rejection could play an important role in stimulating the convection processes in the oceans. Moreover, the presence of ice particles in rivers could produce serious damages to hydroelectric facilities, such as the blocking of turbine intakes, or the blockage of hydroelectric reservoirs. Therefore, the experimental and mathematical investigation of ice production has become, during the years, an active field of research.

The aim of this work is to improve the models currently available for the simulation of ice production in turbulent seawater, by means of the development of a multiphase model able to describe all the stages of ice production, overcoming the limitation of previous attempts, see e.g. [36, 42, 24, 40, 41, 21], mainly based on Boussinesq-like approximation. More specifically, in this work we consider the mixture ice-sea water as a dense compressible fluids. We model the behaviour of seawater by means of an equation of state derived from [7], that links seawater density to temperature, salinity and pressure, allowing us to go beyond the Boussinesq approximation. The model is able to reproduce the interaction phenomena occurring between phases when ice volume fraction is large, including in the momentum equations additional terms, related to the drag force between liquid and particles, and to the particle-particle interaction force. For this purpose, the model uses a sophisticated modelling approach, typically adopted for the numerical simulation of multiphase flows of industrial interest [16]. A low-Mach number asymptotic analysis has been performed to investigate the behaviour of the multiphase equations in the incompressible limit. The divergence constraint condition for the velocity field of continuous phase can then been imposed on the zero-Mach number equations by means of a projection method. As a starting point toward the development of an advanced numerical solver implementing our multiphase model, we develop a finite volume solver by means of a projection method based on [4, 19, 20], to be valid under the Boussinesq approximation, i.e. for small ice concentration regime, using the OpenFOAM library.

The paper is organized as follows: section 2 describes the multiphase model equations for the mixture ice-seawater, the non-dimensional form and the asymptotic analysis, whereas section 3 is devoted to the Boussinesq model equations. In section 4 we present the time discretization by projection method, for the Boussinesq model. Section 5 is devoted to the numerical results for a Boussinesq laminar Rayleigh-Bénard convection, for water and for the mixture ice-water, and ice-salt-water.

2 THE MULTIPHASE MODEL EQUATIONS

We now introduce the multiphase model equations according to the Eulerian-Eulerian approach, coupled with a sophisticated modelling approach for the interaction terms between phases, typically adopted for the numerical simulation of multiphase flows of industrial interest. The governing equations proposed here have been derived carrying out a volume averaging considering an averaging volume V such as $l^3 \ll V$, where l denotes the mean distance between the ice particles. We define the density of the mixture ice-seawater as $\rho = \phi_I \rho_I + (1 - \phi_I)\,\rho_w$, in which ϕ_I stands for the ice volume fraction, and ρ_I and ρ_w denote the ice and water density, respectively. In this work we consider the ice density as a constant value. A large number of models for the equation of state for seawater have been proposed over the years in the oceanographic literature. We have focused our attention on those formulations suitable for numerical modelling, see e.g.[6, 15, 14, 33, 32, 29, 23]. Here we propose a reduced form for the equation of state, derived from the equation proposed in [7], that combines the approaches proposed in [15, 23], providing a simplification of the UNESCO formula [33] that has been found to be valid for $-2°C < \theta < 40°C$, $0\ psu < S < 42\ psu$. Our state equation can be written as

$$\rho_w\,(T, S, p) = D_r p + E_r, \tag{1}$$

where the D_r and E_r coefficients stand for $D_r = b_5 TS + b_2 T + b_1$, and $E_r = a_5 TS + a_4 T^2 + a_3 S + a_2 T + a_1 + \rho_0$, $\rho_0 = 1000 kg/m^3$ is a reference density. The coefficients a_i and b_i are given in Table 1. According to the equation 1, the speed of sound is given by $c = [1/D_r]^{1/2}$.

n	a_n	b_n
1	-9.20601×10^{-2}	$+5.07043 \times 10^{-1}$
2	$+5.10768 \times 10^{-2}$	-3.69119×10^{-3}
3	$+8.05999 \times 10^{-1}$	-
4	-7.40849×10^{-3}	-
5	-3.01036×10^{-3}	$+1.75145 \times 10^{-5}$

Table 1: Coefficients of the equation of state

The continuity equations for the liquid and solid phases can be written as

$$\tfrac{\partial}{\partial t}[\,(1 - \phi_I)\,\rho_w] + \tfrac{\partial}{\partial x_i}[\,(1 - \phi_I)\,\rho_w u_i] = S_{mass}, \tag{2}$$

$$\tfrac{\partial}{\partial t}\,(\phi_I \rho_I) + \tfrac{\partial}{\partial x_i}\,(\phi_I \rho_I v_i) = -S_{mass}. \tag{3}$$

where S_{mass} is the source term, defined as

$$S_{mass} = \frac{2\phi_I h}{RL}\,(T_f - T_w)\,, \tag{4}$$

where h is the convective heat transfer coefficient, R stands for the average radius of the ice particles, L is the specific latent heat of fusion, T_w denotes the water temperature and T_f is the freezing temperature. The momentum equations for water and ice read

$$\frac{\partial}{\partial t}\Big[(1 - \phi_I)\,\rho_w u_i\Big] + \frac{\partial}{\partial x_j}\Big[(1 - \phi_I)\,\rho_w u_j u_i\Big] + f^{cor}_{i,j} u_j = -\,(1 - \phi_I)\,\frac{\partial \bar{p}}{\partial x_i} + (1 - \phi_I)\,\frac{\partial \tau_{ij}}{\partial x_j}$$
$$+F^w_i + (1 - \phi_I)\,\bar{\rho}_w g_i + S_{mom}, \tag{5}$$

$$\frac{\partial}{\partial t}\left(\phi_{\mathrm{I}}\rho_{\mathrm{I}}v_i\right)+\frac{\partial}{\partial x_j}\left(\phi_{\mathrm{I}}\rho_{\mathrm{I}}v_jv_i\right)+f^{cor}_{i,j}v_j=-\phi_{\mathrm{I}}\frac{\partial\bar{p}}{\partial x_i}+\phi_{\mathrm{I}}\frac{\partial\tau_{ij}}{\partial x_j}+F^{\mathrm{I}}_i+\phi_{\mathrm{I}}\rho_{\mathrm{I}}g_i-S_{mom}, \tag{6}$$

where the quasi pressure $\bar{p}$ is defined as $\bar{p}=p+\rho_0 gz$, and $\bar{\rho}_{\mathrm{W}}$ stands for $\bar{\rho}_{\mathrm{W}}=\rho-\rho_0$.
F^{W}_i and F^{I}_i can be split in two terms $F^{\mathrm{W}}_i=f^{\mathrm{W},drag}_i+f^{\mathrm{W},\mathrm{I}}_i$ and $F^{\mathrm{I}}_i=f^{\mathrm{I},drag}_i+f^{\mathrm{I},\mathrm{I}}_i$. Here, $f^{\mathrm{W},drag}_i$ and $f^{\mathrm{I},drag}_i$ denote the drag terms between seawater and particles, depending on the relative velocity (u_i-v_i) ; $f^{\mathrm{W},\mathrm{I}}_i$ denotes the shear stress term, analogous to the Reynolds stress in a single phase flow, that accounts for the velocity deviations that can occur on the seawater flow around a single particle; $f^{\mathrm{I},\mathrm{I}}_i$ denotes the particle-particle interaction term. S_{mom} is the source term and $f^{cor}_{i,j}$ is an antisymmetric tensor such that $f^{cor}_{i,j}u_j$ and $f^{cor}_{i,j}v_j$ represent the Coriolis rotational forces on water and ice, respectively.
The momentum source term can be expressed as

$$S_{mom}=\frac{2\phi_{\mathrm{I}}h}{RL}\left(T_f-T_{\mathrm{W}}\right)v_i. \tag{7}$$

The liquid-solid drag term satisfies $f^{\mathrm{W},drag}_i=-f^{\mathrm{I},drag}_i$. Following the approach proposed in [17], for gas-solid fluidized bed, $f^{\mathrm{W},drag}_i$ can be written as $f^{\mathrm{W},drag}_i=K_D\left(u_i-v_i\right)$, where K_D stands for the two-phase drag coefficient. For the evaluation of K_D we refer to [17], in which K_D is defined as a function of a drag coefficient C_D, and the relative Reynolds number $Re_s=\left(\rho_{\mathrm{W}}D\mid v_i-u_i\mid\right)/\mu_{\mathrm{W}}$. A large number of models have been proposed during the years for the evaluation of the drag terms, see e.g. [43], for gas-solid multiphase flows, and [17, 43, 45], for the evaluation of the liquid-solid drag in the framework of pipeline slurry flows, fluidized bed reactors, as well as in other chemical reacting systems, see e.g. [27, 22, 39, 46, 11, 37], or in numerical modelling of volcanic eruptions, see e.g. [8, 9]. The term $f^{\mathrm{W},\mathrm{I}}_i$ is analogous to the Reynolds stress in a single phase flow. Following the approach reported in [12], we can define $f^{\mathrm{W},\mathrm{I}}_i$ by means of an effective stress τ^e_{ij} such that

$$f^{\mathrm{W},\mathrm{I}}_i=\frac{\partial}{\partial x_j}\left(\left(1-\phi_{\mathrm{I}}\right)\tau^e_{ij}\right), \tag{8}$$

where the effective shear stress, τ^e_{ij}, is related to the turbulence parameters of the flow. The evaluation of τ^e_{ij}, is often carried out by means of eddy viscosity models. The particle-particle interaction term can be written as,

$$f^{\mathrm{I},\mathrm{I}}_i=\phi_{\mathrm{I}}\frac{\partial}{\partial x_j}\left(-p_s\delta_{ij}+\tau_{s,ij}\right). \tag{9}$$

The terms p_s and $\tau_{s,ij}$ stand for the solid pressure and the solid shear stress tensor, respectively. p_s and $\tau_{s,ij}$ can be evaluated as function of the granular temperature Θ, according to the kinetic theory, originally applied by Bagnold [2] to this purpose. Starting from [2], several efforts have been devoted over the years to the development of the kinetic theory, see e.g [35, 38, 30, 26]. Here we mainly refer to the formulations proposed in [16, 30, 25]. Following this theory, an additional transport equation for the kinetic energy of the fluctuating motion of the dispersed phase, also called granular temperature Θ, is required. The kinetic energy associated with the particle velocity fluctuation, can be expressed as $\Theta=\frac{1}{3}\langle C\rangle^2$, where C is the deviation of the particle velocity from the mean velocity. The operator $\langle\ \rangle$ denotes the mean value based on the Gaussian distribution. The equation for the granular temperature can be written, following [16], as

$$\frac{3}{2}\left[\frac{\partial}{\partial t}\left(\rho_I \phi_I \Theta\right) + \frac{\partial}{\partial x_i}\left(\rho_I \phi_I v_i \Theta\right)\right] = \left[-p_s \delta_{ij} + \tau_{s,ij}\right]\frac{\partial v_i}{\partial x_j} - \frac{\partial}{\partial x_i}\left(k_\Theta \frac{\partial \Theta}{\partial x_i}\right) - \Gamma_\Theta. \quad (10)$$

Here, p_s, $\tau_{s,ij}$, k_θ, Γ_θ stand for the solid pressure, the solid shear stress tensor, the coefficient of conductivity of granular temperature, and the dissipation term, respectively, and can be calculated as functions of Θ using different approaches, see e.g. [30, 16, 44, 25].

The transport equation for the water temperature can be written as follows

$$\frac{\partial}{\partial t}\Big[\left(1-\phi_I\right)T_\mathrm{w}\Big] + \frac{\partial}{\partial x_i}\Big[\left(1-\phi_I\right)u_i T_\mathrm{w}\Big] = \frac{\partial}{\partial x_i}\left(\left(1-\phi_I\right)k_t \frac{\partial T_\mathrm{w}}{\partial x_i}\right) + \phi_I \lambda_t \left(T_I - T_\mathrm{w}\right) + S_T. \quad (11)$$

The parameter λ_t is defined as $\lambda_t = \frac{3h}{c_p \rho_W R}$. S_T is the source term, defined as

$$S_T = \frac{2h\phi_I}{R c_p \rho_\mathrm{w}}\left(T_f - T_\mathrm{w}\right), \quad (12)$$

where c_p stands for the water specific heat at constant pressure.

The equation for the salinity S is formulated as

$$\frac{\partial}{\partial t}\Big[\left(1-\phi_I\right)S\Big] + \frac{\partial}{\partial x_i}\Big[\left(1-\phi_I\right)S u_i\Big] = \frac{\partial}{\partial x_i}\left(\left(1-\phi_I\right)k_s \frac{\partial S}{\partial x_i}\right) + S_{sal}, \quad (13)$$

where k_s is the salt diffusivity, and S_{sal} is the source term,

$$S_{sal} = \frac{2hS_v \phi_I \rho_I}{RL\rho_\mathrm{w}}\left(T_f - T_\mathrm{w}\right), \quad (14)$$

where S_v denotes the increase of salinity due to the freezing, that can be defined as $S_v = m_s / \left[V\left(1 - \frac{\phi_I \rho_I}{\rho}\right)\right]$, in which m_s stands for the salt mass and V is the volume of the water-ice mixture.

2.1 Non-dimensional form

In order to obtain the non-dimensional form of the governing equations, we consider the vertical length of the computational domain L as the reference length; the temperature gap between upper and lower boundary of the computational domain, ΔT, as temperature scale; the water velocity ,u_∞, as the velocity scale; the characteristic time t^* as temporal scale; the water density, ρ_{w_∞}, as density scale; and p_∞ and S_0, as reference pressure and reference salinity, respectively. We define the following dimensionless parameters,

$$\widetilde{\alpha} = \alpha \Delta T, \;\; \widetilde{S} = \frac{S}{S_0 \alpha \Delta T}, \;\; \widetilde{\Theta} = \frac{\Theta}{u_\infty^2}, \;\; \widetilde{p}_s = \frac{p_s}{\rho_{\mathrm{w}_\infty} u_\infty^2}, \;\; M_\infty = \frac{u_\infty}{c_\infty}, \quad (15)$$

and the f parameter as $f = u_\infty t^*/L$. For simplicity, in the following sections we denote $S_0 \alpha \Delta T$ as S_∞, and ΔT as T_∞. Other dimensionless parameters are the non-dimensional numbers, Reynolds, R_e, Prandtl, P_r, Rayleigh, R_a, and Schmidt, S_{c_s}

$$R_e = \frac{u \rho_\mathrm{w} L}{\mu}, \;\; P_r = \frac{\nu}{k_t}, \;\; R_a = \frac{g\alpha L^3 \Delta T}{k_t \nu}, \;\; S_{c_s} = \frac{\nu}{k_s}, \quad (16)$$

where μ and ν are the dynamic and kinematic viscosity, respectively, k_t is the water thermal diffusivity, α the thermal expansion coefficient, g the gravity acceleration and k_s is the salt diffusivity. The non-dimensional form of the equation of state, Equation 1, yields

$$\widetilde{\rho}_{\mathrm{w}} = D_r^* \widetilde{D}_r \widetilde{p} + E_r^* \widetilde{E}_r, \tag{17}$$

$$D_r^* = \frac{D_{r\infty} p_\infty}{\rho_{\mathrm{w}_\infty}}, \quad E_r^* = \frac{E_{r\infty}}{\rho_{\mathrm{w}_\infty}}, \quad \widetilde{D}_r = \frac{D_r}{D_{r\infty}}, \quad \widetilde{E}_r = \frac{E_r}{E_{r\infty}}. \tag{18}$$

In the following we will work with the non dimensional equations, dropping the ~ sign for simplicity. The non-dimensional mass conservation equations can be written as,

$$\frac{\partial}{\partial t}\Big[(1-\phi_I)\,\rho_{\mathrm{w}}\Big] + f\frac{\partial}{\partial x_i}\Big[(1-\phi_I)\,\rho_{\mathrm{w}} u_i\Big] = S_{mass}, \tag{19}$$

$$\frac{\partial}{\partial t}(\phi_I \rho_I) + f\frac{\partial}{\partial x_i}(\phi_I \rho_I v_i) = -S_{mass}, \tag{20}$$

where the source term yields,

$$S_{mass} = \frac{2\phi_I h t^*}{RL\rho_{\mathrm{w}_\infty}}(T_f - T_{\mathrm{w}}). \tag{21}$$

The non-dimensional momentum equations can be defined as

$$\begin{aligned}\frac{\partial}{\partial t}\Big[(1-\phi_I)\,\rho_{\mathrm{w}} u_i\Big] + f\frac{\partial}{\partial x_j}\Big[(1-\phi_I)\,\rho_{\mathrm{w}} u_j u_i\Big] + f_{Cor} u_i = -f\frac{p_\infty}{\rho_{\mathrm{w}_\infty} c_\infty^2}\frac{1}{M_\infty^2}(1-\phi_I)\frac{\partial \bar{p}}{\partial x_i} + \\ f\frac{1}{Re_\infty}(1-\phi_I)\left(\frac{\partial^2 u_j}{\partial x_j \partial x_i} + \frac{1}{3}\frac{\partial}{\partial x_j}\left(\frac{\partial u_i}{\partial x_i}\right)\right) + F_i^{\mathrm{w}} + f\frac{R_a}{P_r Re_\infty^2 \alpha}(1-\phi_I)\,\bar{\rho}_{\mathrm{w}} - S_{mom},\end{aligned} \tag{22}$$

$$\begin{aligned}\frac{\partial}{\partial t}(\phi_I \rho_I v_i) + f\frac{\partial}{\partial x_j}(\phi_I \rho_I v_j v_i) + f_{Cor} v_i = -f\frac{p_\infty}{\rho_{\mathrm{w}_\infty} c_\infty^2}\frac{1}{M_\infty^2}\phi_I\frac{\partial \bar{p}}{\partial x_i} + \\ f\frac{1}{Re_\infty}\phi_I\left(\frac{\partial^2 u_j}{\partial x_j \partial x_i} + \frac{1}{3}\frac{\partial}{\partial x_j}\left(\frac{\partial u_i}{\partial x_i}\right)\right) + F_i^I + f\frac{R_a}{P_r Re_\infty^2 \alpha}\phi_I \rho_I + S_{mom},\end{aligned} \tag{23}$$

where the source term stands for

$$S_{mom} = \frac{2\phi_I h t^*}{RL\rho_{\mathrm{w}_\infty}}(T_f - T_{\mathrm{w}})\, v_i. \tag{24}$$

The temperature equation for water can be written as

$$\begin{aligned}\frac{\partial}{\partial t}\Big[(1-\phi_I)\,T_{\mathrm{w}}\Big] + f\frac{\partial}{\partial x_i}\Big[(1-\phi_I)\,u_i T_{\mathrm{w}}\Big] = \frac{t^*\nu}{L^2}\frac{\partial}{\partial x_i}\left((1-\phi_I)\frac{1}{P_r}\frac{\partial T_{\mathrm{w}}}{\partial x_i}\right) + \\ \phi_I t^* \lambda_t (T_I - T_{\mathrm{w}}) + S_T.\end{aligned} \tag{25}$$

The source term is given by

$$S_T = \frac{2ht^*\phi_I}{Rc_p \rho_{\mathrm{w}} \rho_{\mathrm{w}_\infty}}(T_f - T_{\mathrm{w}}). \tag{26}$$

The non-dimensional transport equation for salinity can be written as,

$$\frac{\partial}{\partial t}\Big[(1-\phi_I)\,S\Big]+f\frac{\partial}{\partial x_i}\Big[(1-\phi_I)\,Su_i\Big]=f\frac{\partial}{\partial x_i}\left((1-\phi_I)\,\frac{1}{ScRe_\infty}\frac{\partial S}{\partial x_i}\right)+S_{sal}, \tag{27}$$

$$S_{sal}=\frac{2ht^* S_v\phi_I\rho_I\rho_{\mathrm{w}_\infty}}{RLS_\infty\rho_{\mathrm{w}}}\left(T_f-T_{\mathrm{w}}\right). \tag{28}$$

Finally, for granular temperature, the non dimensional form yields,

$$\frac{3}{2}\Big[\frac{\partial}{\partial t}\left(\rho_I\phi_I\Theta\right)+f\frac{\partial}{\partial x_i}\left(\rho_I\phi_I v_i\Theta\right)\Big]=\left[-fp_s\delta_{ij}+\tau_{s,ij}\right]\frac{\partial v_i}{\partial x_j}-\frac{\partial}{\partial x_i}\left(k_\Theta\frac{\partial\Theta}{\partial x_i}\right)-\Gamma_\Theta. \tag{29}$$

2.2 Low-Mach number asymptotic analysis

To investigate the behaviour of the multiphase equations in the incompressible limit, we have expanded each flow variables as e.g., the pressure,

$$p\left(x,t,M_\infty\right)=p^{(0)}+M_\infty^2 p^{(2)}\left(x,t,M_\infty\right). \tag{30}$$

For simplicity, here we report only the zero-Mach number equation for seawater density, Equation 17, the zero-Mach number equation for mass concentration, Equation 19, and the leading and the zero-order equations for momentum, Equations 22 and . The other zero-Mach number equations follow the non-dimensional representation, with all the variables evaluated at the zero-order. The non-dimensional equation for seawater density, at order $O\left(M_\infty^0\right)$, is derived as:

$$\rho_{\mathrm{w}}^{(0)}=D_r^*\left(D_r^{(0)}p^{(0)}\right)+E_r^*E_r^{(0)}, \tag{31}$$

where the coefficients $D_r^{(0)}$ and $E_r^{(0)}$ are functions of the zero-order temperature and salinity, see the Appendix A for the detailed expression of each coefficient. The water mass conservation at order $O\left(M_\infty^0\right)$ yields

$$\frac{\partial}{\partial t}\Big[\left(1-\phi_I^{(0)}\right)\rho_{\mathrm{w}}^{(0)}\Big]+f\frac{\partial}{\partial x_i}\Big[\left(1-\phi_I^{(0)}\right)\rho_{\mathrm{w}}^{(0)}u_i^{(0)}\Big]=S_{mass}^{(0)}. \tag{32}$$

The zero-order ice mass conservation is given similarly. The water and ice momentum equations at the leading order $O\left(M_\infty^{-2}\right)$ yield

$$\frac{\partial\bar{p}^{(0)}}{\partial x_i}=0, \tag{33}$$

therefore, according to the definition of quasi-pressure $\bar{p}^{(0)}$, we obtain

$$\frac{\partial p^{(0)}}{\partial x}=\frac{\partial p^{(0)}}{\partial y}=0, \tag{34}$$

$$\frac{\partial p^{(0)}}{\partial z}=-\rho_0 g. \tag{35}$$

The water momentum equation at order $O\left(M_\infty^0\right)$ yields:

$$\frac{\partial}{\partial t}\left[\left(1-\phi_{I}^{(0)}\right)\rho_{W}^{(0)}u_i^{(0)}\right]+f\frac{\partial}{\partial x_j}\left[\left(1-\phi_{I}^{(0)}\right)\rho_{W}^{(0)}u_j^{(0)}u_i^{(0)}\right]+f_{Cor}^{(0)}u_i^{(0)}=$$
$$-f\frac{p_\infty}{\rho_{W_\infty}c_\infty^2}\left(1-\phi_{I}^{(0)}\right)\frac{\partial\bar{p}^{(2)}}{\partial x_i}+f\frac{1}{Re_\infty}\left(1-\phi_{I}^{(0)}\right)\left(\frac{\partial^2 u_j^{(0)}}{\partial x_j\partial x_i}+\frac{1}{3}\frac{\partial}{\partial x_j}\left(\frac{\partial u_i^{(0)}}{\partial x_i}\right)\right)+$$
$$F_i^{W(0)}+f\frac{R_a}{P_r R_{e_\infty}^2\alpha}\left(1-\phi_{I}^{(0)}\right)\bar{\rho}_{W}^{(0)}-S_{mom}^{(0)}. \tag{36}$$

The ice momentum equation at order $O\left(M_\infty^0\right)$ can be similarly derived. Using the continuity equation, Equation 32, and assuming $f=1$, the following constraint on the divergence of the water velocity is obtained

$$\nabla\cdot u_i^{(0)}=\frac{1}{\left(1-\phi_{I}^{(0)}\right)\rho_{W}^{(0)}}\left[-\frac{D}{Dt}\left(1-\phi_{I}^{(0)}\right)\rho_{W}^{(0)}+S_{mass}^{(0)}\right], \tag{37}$$

where $\frac{D}{Dt}\left(1-\phi_{I}^{(0)}\right)\rho_{W}^{(0)}$ can be written as

$$\frac{D}{Dt}\left(1-\phi_{I}^{(0)}\right)\rho_{W}^{(0)}=\left(1-\phi_{I}^{(0)}\right)\frac{D\rho_{W}^{(0)}}{Dt}-\rho_{W}^{(0)}\frac{D\phi_{I}^{(0)}}{Dt}. \tag{38}$$

Using the zero-oder ice mass conservation, $\frac{D\phi_I^{(0)}}{Dt}$ can be obtained as

$$\frac{D\phi_{I}^{(0)}}{Dt}=-\frac{S_{mass}^{(0)}}{\rho_{I}^{(0)}}-\phi_{I}^{(0)}\frac{\partial v_i^{(0)}}{\partial x_i}, \tag{39}$$

and $\frac{D\rho_W^{(0)}}{Dt}$ can be derived as

$$\frac{D\rho_{W}^{(0)}}{Dt}=\left.\frac{\partial\rho_{W}^{(0)}}{\partial S^{(0)}}\right|_{T_{W}^{(0)},p^{(0)}}\frac{DS^{(0)}}{Dt}+\left.\frac{\partial\rho_{W}^{(0)}}{\partial T_{W}^{(0)}}\right|_{S^{(0)},p^{(0)}}\frac{DT_{W}^{(0)}}{Dt}+\left.\frac{\partial\rho_{W}^{(0)}}{\partial p^{(0)}}\right|_{T_{W}^{(0)},S^{(0)}}\frac{Dp^{(0)}}{Dt}, \tag{40}$$

in which all the partial derivative can be evaluated by means of the equation of state, whereas $\frac{DS^{(0)}}{Dt}$ and $\frac{DT_W^{(0)}}{Dt}$ can be derived using the zero-order temperature and salinity equations, respectively, and $\frac{Dp^{(0)}}{Dt}$ can be evaluated considering the Equation 33, see the Appendix A for the complete derivation of these terms. The divergence constraint can then be rewritten as

$$\nabla\cdot u_i^{(0)}=\frac{1}{\left(1-\phi_{I}^{(0)}\right)\rho_{W}^{(0)}}\left(-\phi_{I}^{(0)}\frac{\partial v_i^{(0)}}{\partial x_i}+\frac{1}{\rho_{W}^{(0)}}\left(1-\frac{\rho_{W}^{(0)}}{\rho_{I}}\right)S_{mass}^{(0)}\right)-\frac{1}{\rho_{W}^{(0)}}\frac{D\rho_{W}^{(0)}}{Dt}. \tag{41}$$

The zero-order equations coupled with the divergence constraint, Equation 41, can then be discretized in time using a projection method, and the divergence constraint will be used to enforce the mass conservation and the equation of state.

3 BOUSSINESQ APPROXIMATION OF THE MULTIPHASE MODEL EQUATIONS

Here we present the Boussinesq approximation for the multiphase equations introduced in the previous sections. This is a starting point for the development of a finite volume multiphase solver, based on the aforementioned multiphase model. The Boussinesq approximation, indeed, allows us to model the initial stage of the ice production phenomena, frazil-ice, in which the ice volume fraction typically does not exceed 10^{-3}. The formulation reported here follows the approach presented in [1]. According to the Boussinesq approximation, the seawater density can be expressed by means of the following linearized equation of state, see e.g. [21]

$$\rho_{\mathrm{w}} = \rho_0 \left(1 - \beta \left(T - T_0\right) + \beta_s \left(S - S_0\right)\right), \tag{42}$$

in which ρ_0, T_0, S_0, denote the reference density, temperature, and salinity, respectively, whereas β and β_s are the expansion coefficients. Using the Boussinesq approximation, density variations are sufficiently small such that they can be retained only in the buoyancy term of the momentum equation, see e.g [10]. According to such approximation, our multiphase model reduces to a single-phase model, then all the interaction terms and the mass and momentum source terms vanish. Retaining only the equations for water, and assuming the water density to be constant, except in the buoyancy term, the governing equations reduce to

$$\frac{\partial u_i}{\partial x_i} = 0, \tag{43}$$

$$\frac{\partial u_i}{\partial t} + \frac{\partial \left(u_i u_j\right)}{\partial x_j} = -\frac{\partial \pi}{\partial x_i} + \frac{1}{Re}\frac{\partial^2 u_i}{\partial x_j^2} - g_i \left(\beta \left(T - T_0\right) - \beta_s \left(S - S_0\right)\right), \tag{44}$$

$$\frac{\partial T_{\mathrm{w}}}{\partial t} + \frac{\partial \left(u_i T_{\mathrm{w}}\right)}{\partial x_i} = \frac{\partial}{\partial x_i}\left(k_t \frac{\partial T_{\mathrm{w}}}{\partial x_i}\right) + S_T, \tag{45}$$

where π denotes the quasi-pressure, defined as $\pi = \left(p - \rho_0 g\right)/\rho_0$, according to the treatment proposed in [13]. The source term for temperature, S_T, is given by

$$S_T = \frac{2h}{R c_p \rho_{\mathrm{w}} \rho_{\scriptscriptstyle I}} \rho C_{\scriptscriptstyle I} \left(T_f - T_{\mathrm{w}}\right), \tag{46}$$

where $C_{\scriptscriptstyle I}$ denotes the ice mass concentration, and ρ stands for the density of the mixture, given by

$$\rho = \left(\frac{C_{\scriptscriptstyle I}}{\rho_{\scriptscriptstyle I}} + \frac{\left(1 - C_{\scriptscriptstyle I}\right)}{\rho_{\mathrm{w}}}\right)^{-1}. \tag{47}$$

We can describe the scalar transport phenomena for the ice mass concentration $C_{\scriptscriptstyle I}$, by means of the following equation

$$\frac{\partial}{\partial t}\left(\rho C_{\scriptscriptstyle I}\right) + \frac{\partial}{\partial x_i}\left(\rho C_{\scriptscriptstyle I} u_i\right) = -\omega_{r_i}\frac{\partial \left(\rho C_{\scriptscriptstyle I}\right)}{\partial x_i} + k_{\scriptscriptstyle I}\frac{\partial}{\partial x_i}\left(\rho \frac{\partial C_{\scriptscriptstyle I}}{\partial x_i}\right) + S_{C_I}, \tag{48}$$

where $k_{\scriptscriptstyle I}$ is the ice thermal diffusivity, and S_{C_I} denotes the source term, that can be expressed as

$$S_{C_I} = \frac{2h}{R L \rho_{\scriptscriptstyle I}} \rho C_{\scriptscriptstyle I} \left(T_f - T_{\mathrm{w}}\right). \tag{49}$$

The Equation 48 is derived assuming the ice velocity as $u_{\scriptscriptstyle I} = u + \omega_r$, where u is the velocity of the mixture, and $\omega_r = (0, v_r, 0)$ stands for the rise velocity, related to buoyancy forces. In this work we left ω_r as a free parameter, to be evaluated according to experimental investigations, see e.g. [34]. The transport equation for salinity S can be written as

$$\frac{\partial S}{\partial t} + \frac{\partial}{\partial x_i}(Su_i) = \frac{\partial}{\partial x_i}\left(k_s \frac{\partial S}{\partial x_i}\right) + S_{sal}, \tag{50}$$

where k_s is the salt diffusivity, and S_{sal} is the source term, defined as follows

$$S_{sal} = \frac{2h}{RL\rho_{\mathrm{w}}} S_v \rho C_I (T_f - T_{\mathrm{w}}), \tag{51}$$

where the increase of salinity due to the freezing, S_v, stands for $S_v = m_s / [V(1 - C_I)]$, in which m_s is the salt mass and V is the volume of the water-ice mixture.

4 TIME DISCRETIZATION BY PROJECTION METHOD FOR BOUSSINESQ FLOWS

The Boussinesq simplification of the Navier-Stokes equations is integrated in time by a second order projection method constructed in order to have good kinetic energy conservation. Space discretization is performed by a cell-centered second order finite volume approach, while time evolution is computed by using the trapezoidal rule in a colocated non-incremental approximate projection method. The overall method is characterized by a limited amount of numerical dissipation, similarly to [19], and thus it forms an appropriate framework for developing future variants to be applied in direct and large-eddy simulations. An alternative projection approach for density variable flows is reported in [5]. Here we present only a brief overview of the numerical methodology, thus postponing a complete discussion of the projection method elsewhere.

The discretization of the evolution equations under the Boussinesq approximation involves several steps. All the primitive quantities are defined as cell averages at cell center of mass and at integer time steps, while only the quasi-pressure π is defined at cell centers and at half-times, similarly to [3]. Here we denote with A_f the area of cell faces, with $n_{f,i}$ the face normal unit vector and with $\overline{(\cdot)}^f$ the interpolation operator acting on cell centered quantities to construct face centered quantities.

Step 1. – The face normal velocities $U^n = \overline{u_i^n}^f n_{f,i}$ are extrapolated in time using second order Adams-Bashforth

$$U^{n+1,\star} = \frac{3}{2}U^n - \frac{1}{2}U^{n-1}, \tag{52}$$

which will be consistent with the incompressibility condition if the face normal velocities from the previous time steps are divergence-free. For the construction of the evolution equation for the ice concentration the face normal mass fluxes $m^n = \overline{\rho^n}^f \, \overline{(u_i^n + \omega_{r,i})}^f n_{f,i}$ are constructed in a similar manner

$$m^{n+1,\star} = \frac{3}{2}m^n - \frac{1}{2}m^{n-1}, \tag{53}$$

accordingly:

$$\rho^{n+1} = \frac{3}{2}\rho^n - \frac{1}{2}\rho^{n-1}. \tag{54}$$

Step 2. – The temperature equation is integrated implicitly by the trapezoidal rule

$$\begin{aligned}\frac{T^{n+1} - T^n}{\Delta t} = \; & -\tfrac{1}{2}\left[D\left(U^{n+1,\star}\,\overline{T^{n+1}}^f\right) + D\left(U^{n+1,\star}\,\overline{T^n}^f\right)\right] \\ & +\tfrac{1}{2}\left[L_{k_t}(T^{n+1}) + L_{k_t}(T^n)\right] + S_T^{n+1/2},\end{aligned} \tag{55}$$

where we introduced the discrete second-order divergence operator D, approximating the divergence at cell centers from face centered quantities, and the discrete second order operator L_{k_t}, approximating $\frac{\partial}{\partial x_j}\left(k_t \frac{\partial T}{\partial x_j}\right)$ at cell centers from cell centered quantities, in which we silently introduce the interpolation $\overline{k_t}^f$. This allows to construct the buoyancy terms in the other equations.

Step 3. – The salinity equation is integrated implicitly by the trapezoidal rule as well

$$\begin{aligned}\frac{S^{n+1}-S^n}{\Delta t} = & -\tfrac{1}{2}\left[D\Big(U^{n+1,\star}\,\overline{S^{n+1}}^f\Big)+D\Big(U^{n+1,\star}\,\overline{S^n}^f\Big)\right] \\ & +\tfrac{1}{2}\left[L_{k_S}(S^{n+1})+L_{k_S}(S^n)\right]+S_S^{n+1/2},\end{aligned} \tag{56}$$

where the discrete operator L_{k_S} approximates $\frac{\partial}{\partial x_j}\left(k_S \frac{\partial S}{\partial x_j}\right)$. Successively the ice concentration equation is integrated by

$$\begin{aligned}\frac{\rho^{n+1}C^{n+1}-\rho^n C^n}{\Delta t} = & -\tfrac{1}{2}\left[D\Big(m^{n+1,\star}\,\overline{C^{n+1}}^f\Big)+D\Big(m^{n+1,\star}\,\overline{C^n}^f\Big)\right] \\ & +\tfrac{1}{2}\left[L_{k_I\rho^{n+1}}(C^{n+1})+L_{k_I\rho^n}(C^n)\right]+S_I^{n+1/2},\end{aligned} \tag{57}$$

where the discrete operator $L_{k_I\rho^n}$ approximates $\frac{\partial}{\partial x_j}\left(k_I \rho^n \frac{\partial C}{\partial x_j}\right)$ to second order accuracy.

Step 4. – The momentum equation is integrated by the trapezoidal rule, thus obtaining a predicted velocity field $u_i^{n+1,\star}$ which is not generally divergence-free

$$\begin{aligned}\frac{u_i^{n+1,\star}-u_i^n}{\Delta t} = & -\frac{1}{2}\left[D\Big(U^{n+1,\star}\,\overline{u_i^{n+1,\star}}^f\Big)+D\Big(U^{n+1,\star}\,\overline{u_i^n}^f\Big)\right] \\ & +\frac{1}{2}\left[L_\nu\Big(u_i^{n+1,\star}\Big)+L_\nu\Big(u_i^n\Big)\right]-G_i\Big(\pi^{n-1/2}\Big) \\ -\frac{1}{2}\,g_i\Big[\beta\Big(\Big(T^{n+1}-T_0\Big)+(T^n-T_0)\Big) & -\beta_s\Big(\Big(S^{n+1}-S_0\Big)+(S^n-S_0)\Big)\Big]\end{aligned} \tag{58}$$

where we introduced the discrete second-order gradient operator G_i approximating the gradient at cell centers from cell centered quantities by the discrete Gauss theorem applied on $\overline{\pi^{n-1/2}}^f$.

Step 5. – The term containing $\pi^{n-1/2}$ is removed from the predicted velocity field

$$u_i^{n+1,\star\star}=u_i^{n+1,\star}+\Delta t\;G_i\Big(\pi^{n-1/2}\Big) \tag{59}$$

in order to construct a non-incremental projection step (i.e., a Poisson equation on $\pi^{n+1/2}$ rather than on $\pi^{n+1/2}-\pi^{n-1/2}$).

Step 6. – The Poisson equation is solved for the unknown $\pi^{n+1/2}$ required to update the divergence-free face normal velocities

$$L\Big(\pi^{n+1/2}\Big)=\frac{1}{\Delta t}D\Big(\overline{u_i^{n+1,\star\star}}^f\Big)\,. \tag{60}$$

Here homogeneous Neumann boundary conditions are applied to the discrete second order laplacian operator L, which are responsible for the preservation of the initial normal gradient of π^0 at the boundaries (see, e.g., [18]).

Step 7. – The predicted and face normal velocities are respectively updated according to

$$u_i^{n+1} = u_i^{n+1,\star\star} - \Delta t\, G_i\Big(\pi^{n+1/2}\Big)\,, \tag{61}$$

$$U^{n+1} = \left[\overline{u_i^{n+1,\star\star}}^{f} n_{f,i} - \Delta t\, G_{n_f}\Big(\pi^{n+1/2}\Big)\right]\,, \tag{62}$$

$$m^{n+1} = \left[\overline{\rho^{n+1}}^{f}\ \overline{(u_i^{n+1,\star\star} + \omega_{r,i})}^{f} n_{f,i} - \Delta t\, \overline{\rho^{n+1}}^{f} G_{n_f}\Big(\pi^{n+1/2}\Big)\right]\,, \tag{63}$$

where the discrete second order face normal gradient operator G_{n_f} is introduced, approximating the normal gradient at cell faces from cell centered quantities. The resulting face normal velocities U^{n+1} are divergence-free as required by the convective terms. Tangential boundary conditions on u_i^{n+1} are now directly enforced, since they cannot result naturally from the projection step.

The initial value problem requires initial values of u_i^0 at time $t = 0$ and relative boundary conditions. In our calculations we always started from uniformly zero fields on u_i^0 and π^0 whenever possible, or we started from a velocity field resulting after an initial projection step. As a consequence we implicitly assumed at boundaries the artificial condition $\frac{\partial \pi}{\partial x_i} n_{b,i} = 0$, where $n_{b,i}$ represents the unit vector normal to the boundary.

A numerical solvers called `fsBMA` has been implemented according to this formulation, by means of the OpenFOAM library [47].

5 NUMERICAL RESULTS

In order to validate the full multiphase model we shall proceed step by step. As a first step we consider here a simplified version of the equations, namely the Boussinesq approximation. The time discretization is the same described in the previous section, except for source terms, that have been integrated at first order for simplicity, and for the density of the mixture ρ that has been extrapolated at first order. Our analysis has to be intended as a sensitivity study of the influence of the ice formation process on the behaviour of the velocity and temperature fields, for unsalted and salted water, therefore does not completely reproduce the realistic condition of ice production in seawater. The results we present here are the numerical solutions of a three dimensional laminar Rayleigh-Bénard convection of a Boussinesq fluid. Numerical simulations have been performed using the developed `fsBMA` solver, for water, section 5.1, for the water-ice and water-ice-salt mixture, section 5.2.

5.1 Laminar Rayleigh-Bénard convection for water

Numerical simulations have been performed for $Ra = 2.3 \times 10^4$, using a three dimensional $6D$xDx$6D$ domain, where D denotes the height, discretized by means of a uniform 60x10x60 computational grid and a non-uniform 60x50x60 grid, with the smaller mesh size near the top and bottom walls. The boundary conditions at top and bottom walls are free-slip for velocity. The zero-gradient condition has been imposed at top and bottom for pressure, whereas for the temperature we impose T_t, and T_b, respectively. The boundary conditions for all the lateral boundaries are periodic. The simulations have been carried out using $T_t = 272.15\,[K]$, $T_b = 274.15\,[K]$, and $\beta = 3.6476 \times 10^{-3}\,[1/K]$, $\nu = 1.6438 \times 10^{-6}\,[m^2/s]$, $k_t = 1.3905 \times 10^{-7}\,[m^2/s]$ for the thermal expansion coefficient, kinematic viscosity coefficient, and thermal diffusivity, respectively. The simulations have been performed by imposing an initial random perturbation for the temperature and velocity fields. Numerical results have been compared with those obtained by means of a finite difference numerical code presented in [1], on a non-uniform 60x50x60 grid, locally refined near top and bottom walls.

Figure 1 shows the contours and the isolines for the temperature fields, and the U_y velocity component, in the vertical x, y midplane at $z = 3D$ and in the horizontal x, z midplane, at $y = D/2$, respectively, obtained by means of the non-uniform 60x50x60 grid.

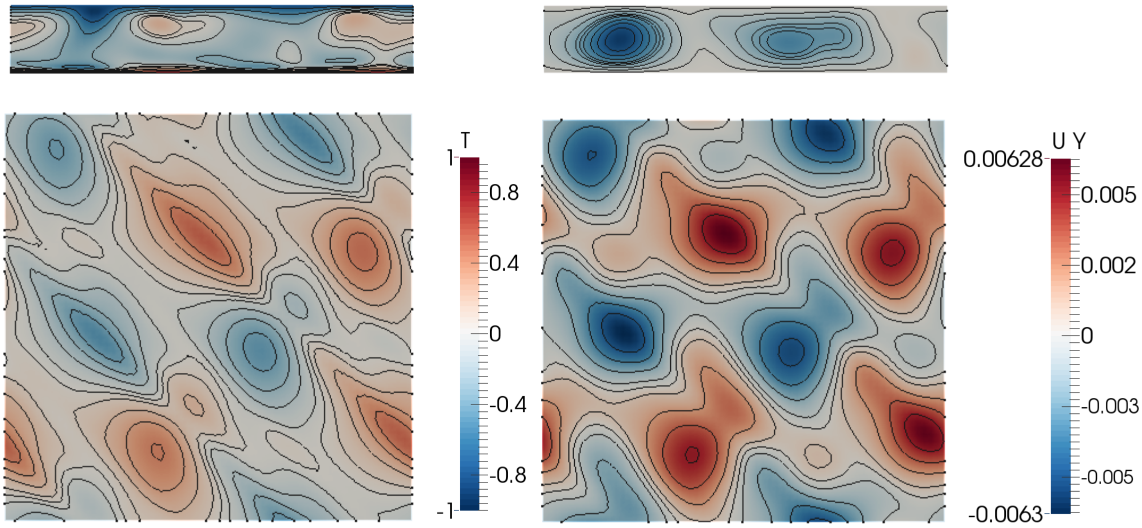

Figure 1: Contours and isolines of temperature, T, left column, and of the U_y velocity component, right column, in the x, y midplane, top row, and in the x, z midplane, bottom row, for water at $Ra = 2.3 \times 10^4$.

Figure 2 shows the comparison between the finite difference code, `FD`, and the developed finite volume solver `fsBMA`, in terms of the time average of the temperature profile, spatially averaged over the x, z plane, and the root mean square of U_y velocity profile, along the y axis.

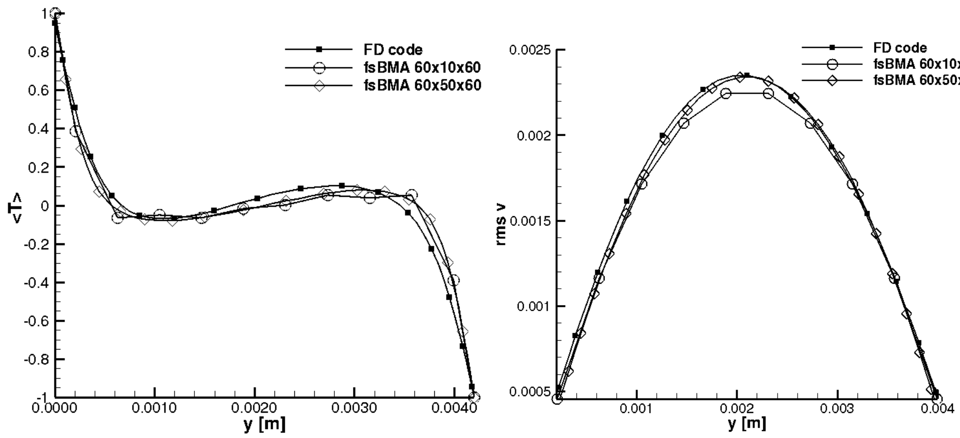

Figure 2: Comparison between the space-time average temperature profiles $< T >$, left plot, and between the root mean square of the U_y component, right plot, along the y axis, obtained with the `FD` code and the `fsBMA` solver.

The profiles in Figure 2 are referred to the 60x50x60 non-uniform mesh for the `FD` solver, and to the 60x10x60 and 60x50x60, uniform and non-uniform mesh, for the `fsBMA` solver. We observe that both the `fsBMA` space-time average profile $< T >$, and the root mean square of the U_y component are in good agreement with the `FD` results. Moreover, the comparison highlights the effects of the grid resolution. The finer non-uniform grid, indeed, allows us to obtain an average temperature profile and a root mean square of U_y velocity that better reproduce the reference `FD` profile, suggesting a convergent trend of the curves increasing the grid resolution.

5.2 Laminar Rayleigh-Bénard convection for the ice-water and the ice-salt-water mixture

The numerical simulations have been carried out following the configuration adopted in the previous section, but now simulating the ice-water and the ice-water-salt mixture. Computations have been performed for both configurations on uniform 60x10x60 grid. We begin our analysis presenting the numerical results of the ice-water simulation. The simulation has been performed imposing on the top and bottom walls a zero gradient condition for the ice mass conservation. The rise velocity has been set $w_r = 0.01 m/s$, according to the experimental investigation reported in [34], moreover the ice thermal diffusivity, the ice density and the particle average radius are, $k_I = 1.18 \times 10^{-6}\,[m^2/s]$, $\rho_I = 917\,[kg/m^3]$, $R = 0.5 \times 10^{-3}\,[m]$, respectively, assuming the frazil-ice particles of disk-like shape. We perform the numerical simulation imposing an initial random perturbation for the ice concentration. Figure 3 shows the behaviour of temperature and ice mass concentration on the x, y and x, z midplanes.

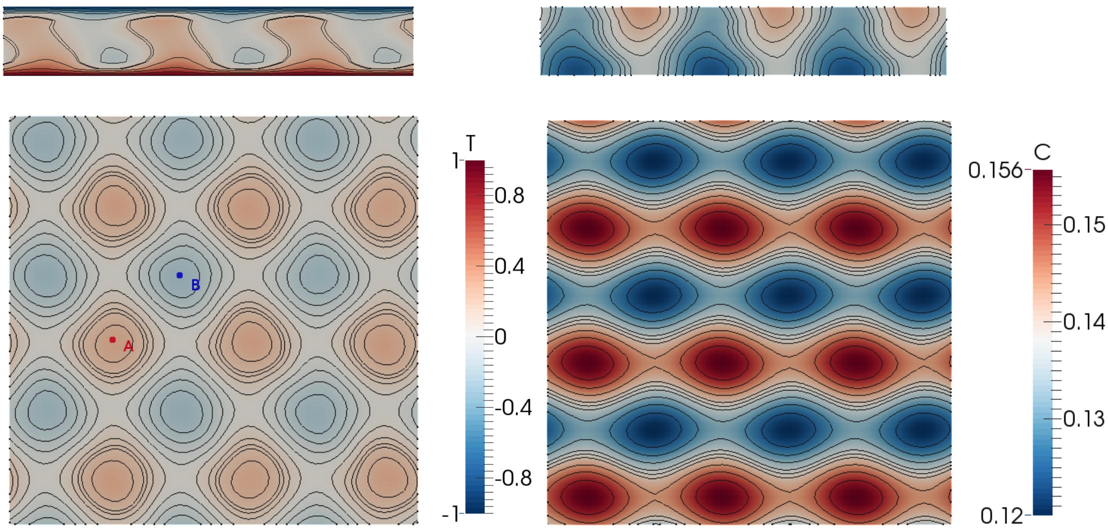

Figure 3: Contours and isolines of temperature, T, left column, and of the ice mass concentration, C, right column, in the x, y midplane, top row, and in the x, z midplane, bottom row, for the ice-water mixture at $Ra = 2.3 \times 10^4$.

Note that on the x, y midplane the distribution of frazil ice concentration follows the trend of the temperature field, showing its maximum values near the zones at lower temperature, whereas the behaviour of frazil ice concentration on the x, z midplane highlights the effects of the transport phenomena due to the U_x and U_y velocity components. The velocity fields on the x, y and x, z midplanes are shown in Figure 4, for each components. In Figure 5 we present the temperature and ice concentration profiles, evaluated along two different vertical lines, A, and B. The A, B lines are located on the x, z plane as shown in Figure 3, left plot.

Starting from the numerical solution obtained for the water-ice mixture, an initial uniform salinity distribution has then been imposed on the entire computational domain. The initial salinity field has been set equal to the reference value $S_0 = 34.5\ psu$, whereas the boundary condition for salinity at top and bottom walls are zero-gradient. The salt diffusivity and the expansion coefficient are $\alpha_s = 0.7 \times 10^{-9}\,[m^2/s]$ and $\beta_s = 7.86 \times 10^{-4}\,[1/psu]$, respectively.

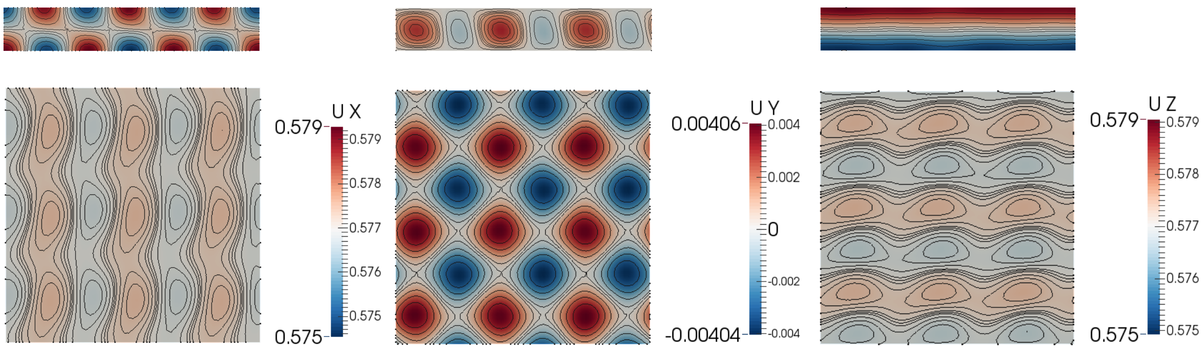

Figure 4: Contours and isolines of U_x, left column, U_y, middle column, and U_z, right column, in the x, y midplane, top row, and in the x, z midplane, bottom row, for the ice-water mixture at $Ra = 2.3 \times 10^4$.

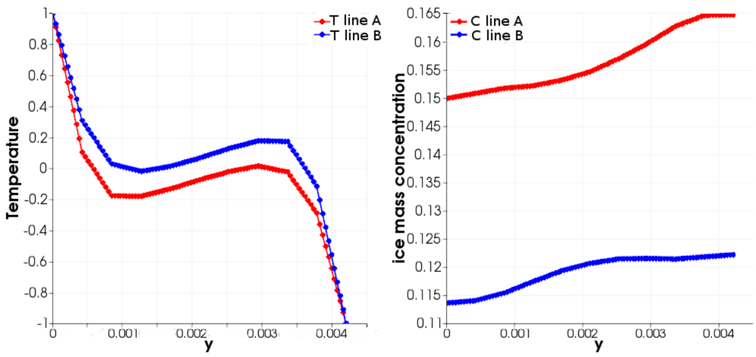

Figure 5: Temperature, left column, and ice mass concentration, right column, profiles along two different vertical lines A, and B, located on the x, z plane as in Figure 3, left plot.

In order to take into account the variation of the freezing temperature due to salinity and width, we define $T_f = T_{f_0} + ah + a_s (S - S_0)$, where a and a_s are the coefficients describing the decrease of T_f with the width, h, and salinity, respectively, and T_{f_0} denotes the freezing temperature of the salted water. The simulation has been performed using $a = 7.61 \times 10^{-4}\,[K/m]$, $a_s = -0.0573\,[K]$, and $T_{f_0} = 271.17\,[K]$. Here we report the numerical results obtained after about 30 hours of simulated time. Figure 6 shows the behaviour of temperature, ice mass concentration and salinity, on the x, y and x, z midplanes, whereas Figure 7 shows the velocity fields on the x, y and x, z midplanes, for each component. We observe from Figures 6 and 7, that on the x, y midplane the larger values of salinity and frazil ice concentration occur close to the top boundary, where temperature shows its minimum values, conversely the salinity and ice concentration reach their minimum values near to the bottom boundary, where the temperature increases. The behaviour of the salinity and the frazil-ice concentration on the x, z midplane highlights the dependence of the salinity on the temperature distribution, and the effects of the velocity field on the transport of ice particles. In Figure 8 we present the temperature, ice mass concentration, and salinity profiles, evaluated along two different vertical lines, C and D. The C, D lines are located on the x, z plane as shown in Figure 6, middle plot.

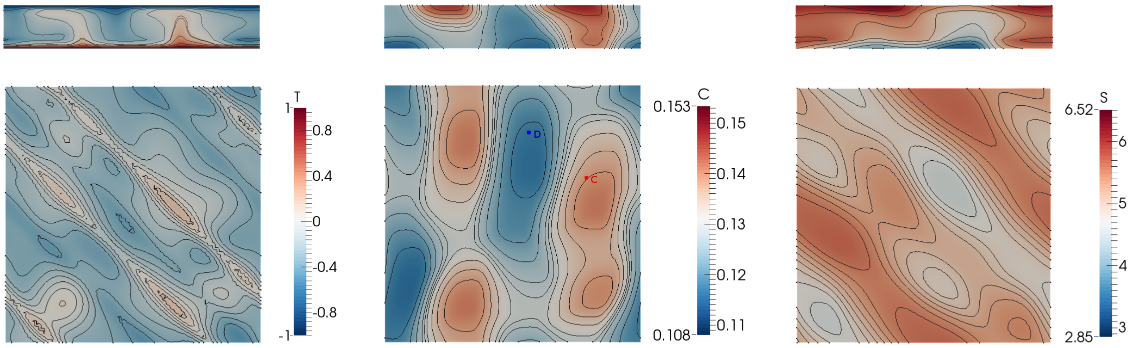

Figure 6: Contours and isolines of temperature, T, left column, ice mass concentration, C, middle column, and salinity, S, right column, in the x, y midplane, top row, and in the x, z midplane, bottom row, for the ice-water-salt mixture at $Ra = 2.3 \times 10^4$.

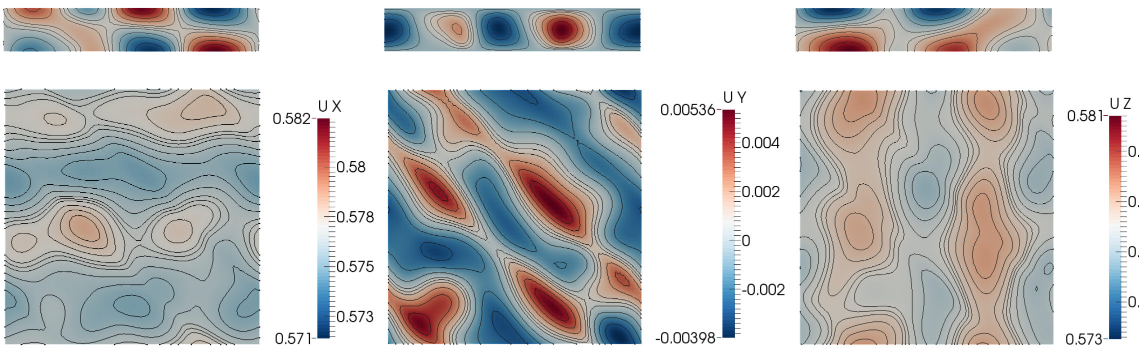

Figure 7: Contours and isolines of U_x, left column, U_y, middle column, and U_z, right column, in the x, y midplane, top row, and in the x, z midplane, bottom row, for the ice-water-salt mixture at $Ra = 2.3 \times 10^4$.

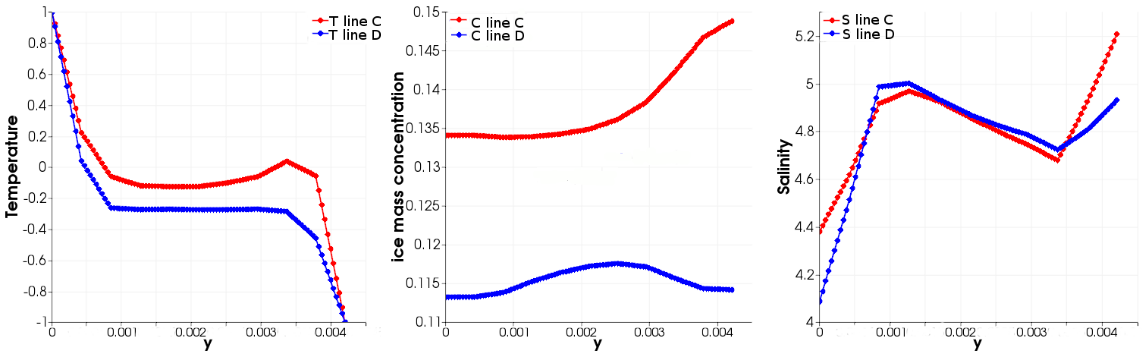

Figure 8: Temperature, left column, ice mass concentration, middle column, and salinity, right column, profiles along two different vertical lines C, and D, located on the x, z plane as in Figure 6, middle plot.

A more comprehensive representation of the convective structures is given in Figure 9, in which we present the three-dimensional contours and isolines of temperature, ice mass concentration and salinity. The isolines are reported on each lateral boundary and on the x, z midplane for $y = D/2$.

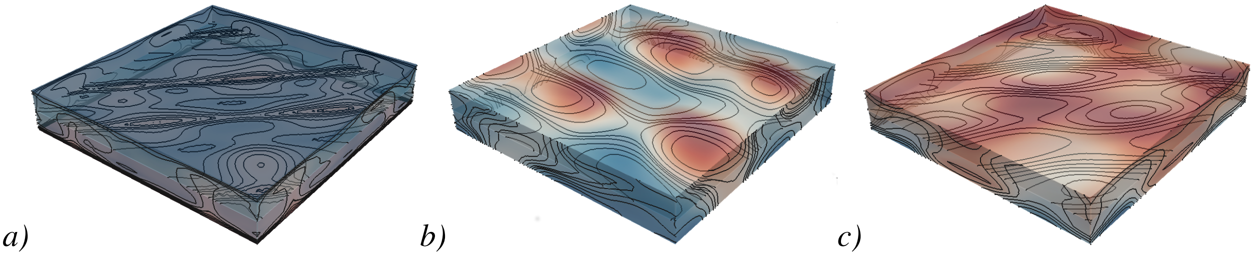

Figure 9: Contours and isolines of temperature, T, a), ice mass concentration, C, b), and salinity, S, c), for the ice-water-salt mixture at $Ra = 2.3 \times 10^4$.

6 CONCLUSION AND FUTURE DEVELOPMENTS

The aim of this work was to improve the predictive capability of the numerical models currently available for the simulation of ice production in seawater, by means of the development of a sophisticated multiphase numerical model able to describe all the stages of ice production, overcoming the limitation of previous attempts, mainly based on the Boussinesq approximation.

We proposed a multiphase model that consider the mixture ice-seawater as a dense compressible fluid, and we modelled the behaviour of seawater density by means of an equation of state, that links density to temperature, pressure and salinity. In order to reproduce the interaction phenomena occurring between phases, we have included in the momentum equations additional terms, derived from the comprehensive modelling approach adopted for the simulation of multiphase flows of industrial interest. A low-Mach number asymptotic analysis has been performed to investigate the behaviour of the multiphase equations in the incompressible limit.

As an initial step of our study, we developed a finite volume numerical solver, by means of the OpenFOAM library, able to reproduce the behaviour of the initial stage of ice formation, according to the Boussinesq approximation. The solver is based on an approximate implicit projection method, according to the colocated version proposed in [4]. The performance of the solver has been assessed by means of the resolution of a Rayleigh-Bénard convection problem, for water and for the mixture ice-seawater. The numerical results obtained for water have been compared with those obtained with a finite difference numerical code.

Ongoing work is focused on the development of an advanced finite volume multiphase solver, for incompressible flows with variable density effects, according to the proposed multiphase approach. We expect that our multiphase model, coupled with the finite volume discretization, could provide an efficient and accurate numerical prediction of all the complex phenomena characterizing the ice production.

Acknowledgements

The present research has been founded by the Italian Ministry of Research and Education in the framework of the PNRA (Italian Program for Antarctic Research) project ”PANACEA The role of frazil and PANcake ice in the mass and energy budgets of the AntartiC sEA ice cover”. The authors gratefully acknowledge the support of Tenova S.p.A.

Appendix A Lagrangian derivative of the zero-Mach number equation of state

Here we present the details of the evaluation of the Lagrangian derivative of the seawater equation of state at order $O\left(M_\infty^0\right)$, used for the derivation of the divergence constraint for the water velocity, Equation 41.
The zero-Mach number equation for the seawater density is given by

$$\rho_W^{(0)} = D_r^*\left(D_r^{(0)} p^{(0)}\right) + E_r^* E_r^{(0)}, \tag{64}$$

where the coefficients are defined as

$$D_r^* = \frac{D_{r_\infty} p_\infty}{\rho_W^{(0)}}, \qquad E_r^* = \frac{E_{r_\infty}}{\rho_W^{(0)}}, \tag{65}$$

$$D_r = \left[b_5 S_\infty T_\infty S^{(0)} T_W^{(0)} + b_2 T_W^{(0)} T_\infty + b_1\right] / D_{r_\infty} \tag{66}$$

$$E_r = \left[a_5 S_\infty T_\infty S^{(0)} T_W^{(0)} + a_4 T_W^2 T_\infty^2 + a_3 S^{(0)} S_\infty + a_2 T_W^{(0)} T_\infty + a_1 + \rho_0\right] / E_{r_\infty} \tag{67}$$

As reported in section 2.2, the Lagrangian derivative of $\rho_W^{(0)}$ can be expressed as

$$\frac{D\rho_W^{(0)}}{Dt} = \left.\frac{\partial \rho_W^{(0)}}{\partial S^{(0)}}\right|_{T_W^{(0)}, p^{(0)}} \frac{DS^{(0)}}{Dt} + \left.\frac{\partial \rho_W^{(0)}}{\partial T_W^{(0)}}\right|_{S^{(0)}, p^{(0)}} \frac{DT_W^{(0)}}{Dt} + \left.\frac{\partial \rho_W^{(0)}}{\partial p^{(0)}}\right|_{T_W^{(0)}, S^{(0)}} \frac{Dp^{(0)}}{Dt}. \tag{68}$$

The partial derivative can be written as

$$\left.\frac{\partial \rho_W^{(0)}}{\partial S^{(0)}}\right|_{T_W^{(0)}, p^{(0)}} = \frac{1}{\rho_W^{(0)}}\left(p_\infty p^{(0)} b_5 S_\infty T_\infty T_W^{(0)} + a_5 S_\infty T_\infty T_W^{(0)} + a_3 S_\infty\right),$$

$$\left.\frac{\partial \rho_W^{(0)}}{\partial T_W^{(0)}}\right|_{S^{(0)}, p^{(0)}} = \frac{1}{\rho_W^{(0)}}\left[p_\infty p^{(0)}\left(b_5 S_\infty T_\infty S^{(0)} + b_2 T_\infty\right) + a_5 S_\infty T_\infty S^{(0)} + 2a_4 T_W T_\infty^2 + a_2 T_\infty\right],$$

$$\left.\frac{\partial \rho_W^{(0)}}{\partial p^{(0)}}\right|_{T_W^{(0)}, S^{(0)}} = \frac{p_\infty}{\rho_W^{(0)}}\left(b_5 S_\infty T_\infty S^{(0)} T_W^{(0)} - b_2 T_W^{(0)} T_\infty + b_1\right).$$

and the Lagrangian derivative $\frac{DS^{(0)}}{Dt}$ and $\frac{DT_W^{(0)}}{Dt}$, can be derived from the zero-Mach number temperature and salinity equations, respectively, as

$$\frac{DS^{(0)}}{Dt} = \frac{1}{\left(1-\phi_I^{(0)}\right)}\left[\frac{\partial}{\partial x_i}\left(\left(1-\phi_I^{(0)}\right)\frac{1}{ScRe_\infty}\frac{\partial S^{(0)}}{\partial x_i}\right) + S_{sal}^{(0)} - S^{(0)}\left(\frac{\partial}{\partial t}\left(1-\phi_I^{(0)}\right) + \frac{\partial}{\partial x_i}\left(1-\phi_I^{(0)}\right)u_i^{(0)}\right)\right] \tag{69}$$

$$\frac{DT_W^{(0)}}{Dt} = \frac{1}{\left(1-\phi_I^{(0)}\right)}\left[\frac{t^*\nu}{L^2}\frac{\partial}{\partial x_i}\left[\left(1-\phi_I\right)\frac{1}{Pr}\frac{\partial T_W^{(0)}}{\partial x_i}\right] + \phi_I^{(0)} t^* \lambda_t^{(0)}\left(T_f - T_W^{(0)}\right) + S_T^{(0)} - T_W^{(0)}\left(\frac{\partial}{\partial t}\left(1-\phi_I^{(0)}\right) + \frac{\partial}{\partial x_i}\left(1-\phi_I^{(0)} u_i^{(0)}\right)\right)\right] \tag{70}$$

In order to evaluate the Lagrangian derivative of pressure at zero-order, $Dp^{(0)}/Dt$, we consider the momentum equation at the leading order $O\left(M_\infty^{-2}\right)$. Since $p^{(0)}$ represent the hydrostatic pressure, for which $\partial p^{(0)}/\partial z = -\rho_0 g$, see Equation 35, and considering $\partial p^{(0)}/\partial t = 0$, the Lagrangian derivative of the seawater density at order $O\left(M_\infty^{0}\right)$, can then be rewritten as

$$\begin{aligned}\frac{D\rho_{\mathrm{w}}^{(0)}}{Dt} = &\frac{1}{\rho_{\mathrm{w}}^{(0)}\left(1-\phi_{\mathrm{I}}^{(0)}\right)}\left(p_\infty p^{(0)} b_5 S_\infty T_\infty T_{\mathrm{w}}^{(0)} + a_5 S_\infty T_\infty T_{\mathrm{w}}^{(0)} + a_3 S_\infty\right)\left[\frac{\partial}{\partial x_i}\left(\left(1-\right.\right.\right.\\ &\left.\left.\phi_{\mathrm{I}}^{(0)}\right)\frac{1}{ScRe_\infty}\frac{\partial S^{(0)}}{\partial x_i}\right) + S_{sal}^{(0)} - S^{(0)}\left(\frac{\partial}{\partial t}\left(1-\phi_{\mathrm{I}}^{(0)}\right) + \frac{\partial}{\partial x_i}\left(1-\phi_{\mathrm{I}}^{(0)}\right)u_i^{(0)}\right)\right] +\\ &\left(b_5 S_\infty T_\infty S^{(0)} T_{\mathrm{w}}^{(0)} - b_2 T_{\mathrm{w}}^{(0)} T_\infty + b_1\right)\left[\frac{t^*\nu}{L^2}\frac{\partial}{\partial x_i}\left[\left(1-\phi_{\mathrm{I}}\right)\frac{1}{Pr}\frac{\partial T_{\mathrm{w}}^{(0)}}{\partial x_i}\right] +\right.\\ &\left.\phi_{\mathrm{I}}^{(0)} t^* \lambda_t^{(0)}\left(T_f - T_{\mathrm{w}}^{(0)}\right) + S_T^{(0)} - T_{\mathrm{w}}^{(0)}\left(\frac{\partial}{\partial t}\left(1-\phi_{\mathrm{I}}^{(0)}\right) + \frac{\partial}{\partial x_i}\left(1-\phi_{\mathrm{I}}^{(0)}\right)u_i^{(0)}\right)\right] -\\ &\frac{p_\infty}{\rho_{\mathrm{w}}^{(0)}}\left(b_5 S_\infty T_\infty S^{(0)} T_{\mathrm{w}}^{(0)} - b_2 T_{\mathrm{w}}^{(0)} T_\infty + b_1\right)u_i^{(0)}\rho_0 g. \end{aligned} \quad (71)$$

REFERENCES

[1] A. Abbà, P. Olla, L. Valdettaro, Numerical Analysis of Frazil Ice Formation in Turbulent Convection, *Progress in Turbulence VI, Proceedings of the iTi Conference on Turbulence, Springer Proceedings in Physics*, 165, 2014.

[2] R.A. Bagnold, Experiments on a gravity-free dispersion of large solid spheres in a Newtonian-fluid under shear, *Proceedings of the Royal Society of London A*, A225, pp. 49-63, 1954.

[3] J.B. Bell, P. Colella, H.M. Glaz, A second-order projection method for the incompressible Navier-Stokes equations, *J. Comput. Phys.*, 85, pp. 257-283, 1989.

[4] J.B. Bell, D.L. Marcus, A second-order projection method for variable-density flows, *J. Comput. Phys.*, 101, pp. 334-348, 1992.

[5] T.Benacchio, W.P. O'Neill, R. Klein, A Blended Soundproof-to-Compressible Numerical Model for Small- to Mesoscale Atmospheric Dynamics, *Mon. Wea. Rev.*, 142, pp. 4416-4438, 2014.

[6] K. Bryan, M.D. Cox, An approximate equation of state for numerical models of ocean circulation., *J. Phys. Oceanogr.*, 2.4, pp. 510-514, 1972.

[7] D. Brydon, S. Sun, R. Bleck, A new approximation of the equation of state for seawater, suitable for numerical ocean models, *JGR-Oceans (1978-2012)*, 104.C1, pp. 1537-1540, 1999.

[8] S. Carcano, L. Bonaventura, A. Neri, T. Esposti Ongaro, A second order accurate numerical model for multiphase underexpanded volcanic jets, *Geophysical Model Development*, 6, pp. 1905- 1924, 2013.

[9] S. Carcano, T. Esposti Ongaro, L. Bonaventura, A. Neri, Influence of grain-size distribution on the dynamics of underexpanded volcanic jets, *J. Volcanol. Geotherm. Res.*, 285, pp. 60-80, 2014.

[10] S. Chandrasekhar, Hydrodynamic and hydromagnetic stability, *Clarendon Press Oxford* 196.1, 1970.

[11] J.T. Cornelissen, F. Taghipour, R. Escudié, N. Ellis, J.R. Grace, CFD modelling of a liquid–solid fluidized bed, *Chem. Eng. Sci.*, 62.22, 6334-6348, 2007.

[12] C.T. Crowe, *Multiphase flows with Droplets and Particles*, CRC Press, Boca Raton, FL., 1998.

[13] J.H. Ferziger, M. Peric, Computational methods for fluid dynamics, *Springer*, 2002.

[14] N.P. Fofonoff, Physical properties of seawater: A new salinity scale and equation of state for seawater, *JGR-Oceans (1978-2012)*, 90.C2, pp. 3332-3342, 1985.

[15] H. Friedrich, S. Levitus, An approximation to the equation of state for sea water, suitable for numerical ocean models., *J. Phys. Oceanogr.*, 2.4, pp. 514-517, 1972.

[16] D. Gidaspow, *Multiphase Flow and Fluidization*, Academic Press, San Diego, CA, 1994.

[17] D. Gidaspow, R. Bezburuah, J. Ding, *Hydrodynamics of circulating fluidized beds, kinetic theory approach*, Potter, O.E., Nicklin, D.J. (Eds.), Fluidization VII. Engineering Foundation, New York, 1992.

[18] J.L. Guermond, P. Minev, J. Shen, An overview of projection methods for incompressible flows, *Computer Methods in Applied Mechanics and Engineering*, 195, pp. 6011-6045, 2006.

[19] F. Ham, G. Iaccarino, Energy conservation in colocated discretization schemes on unstructured meshes, *Ann. Rev. Brief 2004, CTR, NASA, Ames/Stanford Un.*, 2004.

[20] F. Ham, G. Iaccarino, Automatic mesh generation for LES in complex geometries, *Ann. Rev. Brief 2004, CTR, NASA, Ames/Stanford Un.*, 2005.

[21] P.R. Holland, D.L. Feltham, Frazil dynamics and precipitation in a water column with depth-dependent supercooling, *J. Fluid Mech.*, 530, pp. 101-124, 2005.

[22] S. Hosseini, D. Patel, F. Ein-Mozaffari, M. Mehrvar, Study of Solid-Liquid Mixing in Agitated Tanks through Computational Fluid Dynamics Modeling, *Ind. Eng. Chem. Res*, 49.9, pp. 4426-4435, 2010.

[23] D. Jackett, R. Mcdougall, J. Trevor, Minimal adjustment of hydrographic profiles to achieve static stability, *J. Atmos. Oceanic Technol.*, 12.2, pp. 381-389, 1995.

[24] A. Jenkins, A. Bombosch, Modeling the effects of frazil ice crystals on the dynamics and thermodynamics of ice shelf water plumes, *JGR-Oceans (1978-2012)*, 100.C4, pp. 6967-6981, 1995.

[25] J.J. Jenkins, S.B. Savage, A theory for the rapid flow of identical smooth nearly elastic spherical particles, *J. Fluid Mech.*, 130, pp. 187-202, 1983.

[26] P.C. Johnson, R. Jackson, Frictional-collisional constitutive relations for granular materials, with application to plane shearing, *J. Fluid Mech*, 176, pp. 67-93, 1987.

[27] D.R. Kaushal, T. Thinglas, Y. Tomita, S. Kuchii, H. Tsukamoto, CFD modeling for pipeline flow of fine particles at high concentration, *Int. J. Multiph.*, 43, pp. 85-100, 2012.

[28] H.R. Kivisild, *River and lake ice terminology*, International Association for Hydraulic Research, paper 1, 1970.

[29] S. Levitus, G. Isayev, Polynomial approximation to the international equation of state for seawater, *J. Atmos. Ocean. Tech.*, 9.5, pp. 705-708, 1992.

[30] C.K.K. Lun, S.B. Savage, N. Chepurning, Kinetic theories for granular flow: Inelastic particles in Couette flow and singly inelastic particles in a general flow field, *J. Fluid Mech.*, 140, pp. 223-256, 1984.

[31] S. Martin, Frazil ice in rivers and oceans, *Annu. Rev. Fluid Mech.*, 13, pp. 379-397, 1981.

[32] G.L. Mellor, An equation of state for numerical models of oceans and estuaries., *J. Atmos. Oceanic Technol.*, 8.4, pp. 609-611, 1991.

[33] F.J. Millero, A. Poisson, International one-atmosphere equation of state of seawater, *Deep Sea Res. Part A. Oceanogr. Res. Pap.*, 28.6, pp. 625-629, 1981.

[34] B. Morse, M. Richard, A field study of suspented frazil ice particles. *Cold Regions Science and Technology*, 2009.

[35] S.A. Ogawa, A. Umemura, N. Oshima, On the equations of fully fluidized granular materials, *J. Applied Math. Phys. ZAMP*, 31.4, 483-493, 1980.

[36] A. Omstedt, U. Svensson, Modeling supercooling and ice formation in a turbulent Ekman layer, *JGR-Oceans (1978-2012)*, 89.C1, pp. 735-744, 1984.

[37] S. Roy, M.P. Dudukovic, Flow mapping and modeling of liquid-solid risers, *Ind. Eng. Chem. Res.*, 40.23, 5440-5454, 2001.

[38] S.B. Savage, D.J. Jeffrey, The stress tensor in a granular flow at high shear rates, *J. Fluid Mech*, 110, pp. 255-272, 1981.

[39] D. Shi, Z. Luo, Z. Zheng, Numerical simulation of liquid-solid two-phase flow in a tubular loop polymerization reactor, *Powder Technol.*, 198.1, pp. 135-143, 2010.

[40] E.D. Skyllingstad, D.W. Denbo, Turbulence beneath sea ice and leads: A coupled sea ice/large-eddy simulation study, *JGR-Oceans (1978–2012)*, 106.C2, pp. 2477-2497, 2001.

[41] L.H. Smedsrud, A. Jenkins, Frazil ice formation in an ice shelf water plume, *JGR-Oceans (1978–2012)*, 109.C3, 2004.

[42] U. Svensson, A. Omstedt, Numerical simulations of frazil ice dynamics in the upper layers of the ocean, *Cold Reg. Sci. Technol.*, 28.1, pp. 29-44, 1998.

[43] M. Syamlal, W. Rogers, T.J. OBrien, *MFIX documentation: Theory guide*, National Energy Technology Laboratory, Department of Energy, Technical Note DOE/METC-95/1013 and NTIS/DE95000031, 1993.

[44] B.G.M. van Wachem, J.C. Schouten, C.M. van den Bleek, R. Krishna, J.L. Sinclair, Comparative analysis of CFD models of dense gas solid systems, *Journal. Amer. Inst. Chem. Engrs.*, 47, pp. 1035-1051, 2001.

[45] C.Y. Wen, Y.H. Yu, Mechanics of fluidization, *Chem. Eng. Prog. Symp.*, 62, pp. 100-111, 1966.

[46] W. Yan, D. Shi, Z. Luo, Y. Lu, Three-dimensional CFD study of liquid–solid flow behaviors in tubular loop polymerization reactors: The effect of guide vane, *Chem. Eng. Sci.*, 66.18, pp. 4127-4137, 2011.

[47] H.G. Weller, G. Tabor, H. Jasak, C. Fureby, A tensorial approach to computational continuum mechanics using object orientated techniques, *Computers in Physics*, 12.6, pp. 620–631, 1998.